ACS OMEGA

Open Access

http://pubs.acs.org/journal/acsodf

Article

Mechanochemical Synthesis of Graphene Oxide/UiO-66-NH_2 Nanocomposites: Characterization and Fabrication of an Electrochemical Sensor for the Determination of Tetracycline Residues in Milk Samples

Davood Bigdelifam and Mahdi Hashemi*

Cite This: *ACS Omega* 2025, 10, 16184−16193

Read Online

ACCESS | Metrics & More | Article Recommendations | Supporting Information

ABSTRACT: This paper describes a green mechanochemical approach for the synthesis of a graphene oxide-based UiO-66-NH_2 metal organic framework composite (GO/UiO-66-NH_2) for the fabrication of a sensitive electrochemical sensor for the determination of tetracycline (TC) residues in milk samples. The structural and electrochemical characteristics of the GO/UiO-66-NH_2 nanocomposite were investigated by scanning electron microscopy (SEM), X-ray diffraction (XRD), FT-IR spectroscopy, and cyclic voltammetry (CV). Incorporation of UiO-66-NH_2 onto the GO surface can increase the number of effective reaction sites and improve the electrochemical performance of the fabricated sensor. The sensor was simply prepared through drop-casting a GO/UiO-66-NH_2 suspension onto the glassy carbon electrode surface and used for TC determination by differential pulse voltammetry (DPV) as a sensitive analytical method. The fabricated sensor provided a linear calibration over the concentration ranges of 0.02−1.00 μg mL^{-1} (R^2 = 0.9921) and 1.00−40 μg mL^{-1} (R^2 = 0.9932) with a limit of detection of 0.003 μg mL^{-1} using DPV. The proposed sensor was successfully applied to measure the TC residues in different milk samples with satisfying recovery from 94.0 to 105.0%.

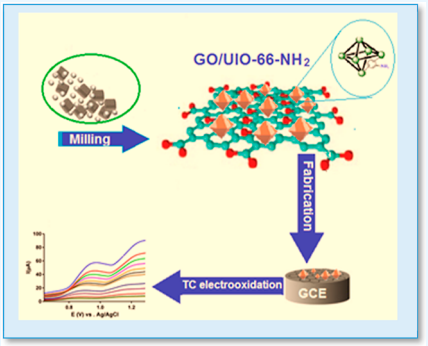

1. INTRODUCTION

Antibiotics are widely used in veterinary medicine for the prevention and treatment of a great number of bacterial infections, control of local and systemic inflammation, such as mastitis and digital dermatitis, as well as a growth promoter in dairy cows.[1] Failure to comply with the correct dosage and time of drug administration can cause a significant amount of the drug to enter the milk, exerting serious harmful effects on public health.[2] Tetracycline (TC, Figure S1) is a broad spectrum antibiotic that is widely used in veterinary treatments and, therefore, is one of the most common drug residues found in dairy products.[3] TC residues in dairy products can result in various health problems, such as induction of allergic reactions, disruption of the normal intestinal flora, increase in antibiotic resistance, and lack of response to antibiotic dosages and development of bacterial resistance.[4] Also, TC residues in raw milk may interfere with the production processes of fermented dairy products, such as yogurt, cheese crud, by inhibiting the activity of normal microflora.[4−6] Accordingly, a maximum residue limit (MRL) of 100 ng/g for TC in milk samples has been recommended by the Joint FAO/WHO Expert Committee on Food Additives (JECFA).[7] The analysis of TC residue in milk samples is of great importance in food quality control to ensure the safe consumption of milk and dairy products. Several analytical methods have been developed for TC determination in milk and food samples, such as high-performance liquid chromatography (HPLC),[8−10] liquid chromatography−mass spectrometry (LC−-MS),[11,12] molecular spectroscopy,[13] fluorimetry,[14] and electrochemical methods.[15−17] Among the different analytical methods, the electrochemical analytical methods have attracted considerable interest in many fields on account of their simple and fast operation, low cost and portability, good sensitivity, variability of the output signals, and high potential for on-site analysis and miniaturization.[18,19]

Recently, metal−organic frameworks (MOFs) are considered to be promising sensing platforms for fabricating electrochemical sensors due to their high porosity and uniform pore size, excellent adsorption performance, reactive capacity, electrocatalytic activity, great stability, film-forming ability, easy functionalization, and controllable synthesis, as pointed out by several reviews.[19−21] However, their application in electrochemical sensing is somewhat limited owing to their intrinsic

Received: November 1, 2024
Revised: February 11, 2025
Accepted: April 11, 2025
Published: April 17, 2025

Scheme 1. Schematic Representation for the Fabrication of GO/UiO-66-NH_2-Based Sensor and Electrochemical Determination of TC

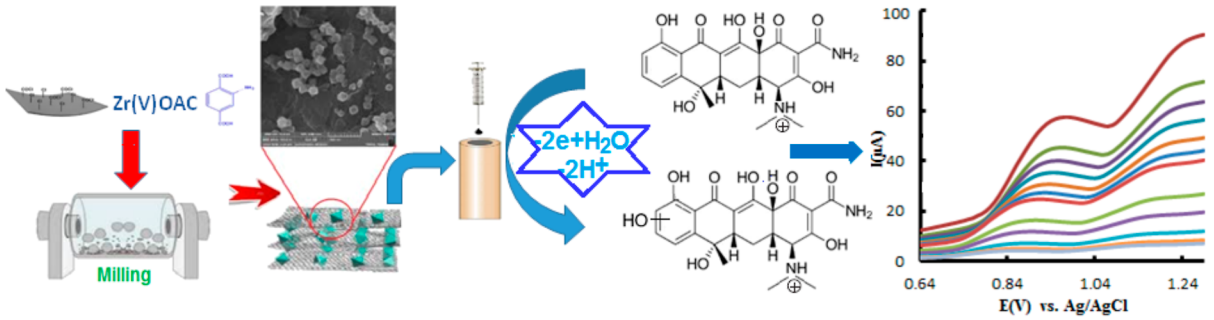

low electronic conductivity due to the nature of the coordination bands in MOFs. The combination of MOFs with conductive materials (such as, carbon-based nanoparticles, metal/metal oxide nanoparticles, and conductive polymers), functionalization of MOFs, thin-film fabrication of MOFs, and synthesis of hybrid MOFs with synergetic interactions are the most common and straightforward strategies to improve the conductivity of MOFs.[22] Among the different MOFs, UiO-66-NH_2 using Zr as the metal center and 2-aminoterephthalic acid as the linker is widely noted for their high catalytic activity, good dispersibility, and outstanding aqueous stability over a wide range of pH.[21] Also, the high affinity of the—NH_2 group to the surface groups of carbon-based supports, such as graphite oxide (GO), can facilitate the uniform incorporation of MOF nanoparticles in the GO surface, resulting in the formation of the stable GO/MOF hybrid composite.[23]

The structural properties of MOFs depend on the synthesis strategy. There are various methods for the synthesis of MOFs, such as hydro/solvothermal, microwave assisted, electrochemical, sonochemical, and mechanochemical methods.[15,16] Mechanochemical processing is a green approach in which chemical reactions occur by grinding or milling without bulk solvents, high temperatures, and/or corrosive reagents. This method provides potential advantages of short reaction time, scalable green approach, and quantitative yields and avoiding corrosive reagents, large quantities of solvent, and high temperatures.[24,25]

In the present work, a new ball milling synthesis method was developed to synthesize the GO/UiO-66-NH_2 composite by cogrinding chlorinated graphene oxide, Zr(IV) acetate, and aminoterphtalic acid. Finally, the GO/UiO-66-NH_2 composite was used as a platform to fabricate an electrochemical sensor to measure TC in different milk samples by differential pulse voltammetry (DPV). The analytical parameters for the detection of TC were investigated and optimized. Scheme 1 shows a step-by-step diagram for the synthetic strategy and fabrication of the GO/UiO-66-NH_2/GCE sensor for the determination of TC. The feasibility of the suggested sensor was studied by the determination of TC in the different milk samples. The proposed electrochemical sensor shows good selectivity, stability, and great potential for TC analysis in various real milk samples.

2. MATERIALS AND METHODS

2.1. Reagents and Apparatus. Zirconium(IV) acetate, 2-aminobenzene-1,4-dicarboxylic acid (NH_2−BDC), phosphorus(V) chloride (PCL_5), potassium ferricyanide ($K_3[Fe(CN)_6]$), potassium ferrocyanide trihydrate ($K_4[Fe(CN)_6]\cdot 3H_2O$), sodium dihydrogen phosphate (NaH_2PO_4), phosphoric acid (H_3PO_4), and disodium hydrogen phosphate (Na_2HPO_4) were purchased from Sigma-Aldrich (St. Louis, MO, USA). Graphene oxide (GO) was purchased from Fine Nano company (Iran). TC stock solution (250.0 μg mL^{-1}) were prepared in phosphate-buffered solutions and kept in a dark glass bottle at 4 °C. A solution of 0.01 mol L^{-1} $[Fe(CN)_6]^{4-/3-}$ containing 0.5 mol L^{-1} KCl in phosphate buffered solution (pH = 2.0) was prepared to determine the performance of the coated electrode. All other solvents and reagents used were of analytical grade and used as received. Double distilled deionized water was also used throughout all experiments.

2.2. Apparatus. The ball milling process was performed by a homemade 80 mL stainless-steel grinding jar (diameter: 13 cm and height: 80 cm), equipped with an inverter control to adjust the rotation speed and stainless-steel balls with different diameters (3, 6, and 8 mm) to create both shear and impact forces for reactants. The characterization studies were performed by scanning electron microscopy (SEM, TESCAN, MIRA3 LMU, Czech Republic), Fourier transform infrared spectroscopy (FTIR, PerkinElmer, Spectrum GX), and X-ray diffraction analysis (XRD, G.N.R, APD 2000 PRO, Italy), respectively. Electrochemical experiments were carried out by a Behpazhoh electrochemical analyzer (model 2066) with a conventional three-electrode system, consisting of a GO/UiO-66-NH_2/GCE working electrode, a platinum wire auxiliary electrode, and a Ag/AgCl (3 M KCl) reference electrode. A Milwaukee pH meter (Model Mi 150, Italy) was used to adjust the pH of the solutions.

2.3. Synthesis of Materials. *2.3.1. Mechanochemical Chlorination of GO.* Graphene oxide (1 g) and phosphorus (V) chloride (5 g, 24 mmol) were mixed and then transferred to a stainless-steel grinding jar with 60 stainless-steel grinding balls with different diameters (3 × 20 balls, each with diameters of 3, 6, and 8 mm). Then, the jar was sealed, and a milling process was performed at 300 rpm for 1 h to ensure product synthesis and prevent any damage to the graphene basal planes. The ball-to-powder mass ratio was consistently kept at about 16:1 for providing enough mechanical energy and a suitable surface area for the reaction. The resulting product was gently washed two times with 15 mL of THF in a beaker and after centrifugation dried in vacuum at 60 °C for 4 h.

2.3.2. Mechanochemical Synthesis of GO/UiO-66-NH_2 and UiO-66-NH_2. In the first step, NH_2−BDC (1 g, 5.5 mmol) and chlorinated GO (1 g) were placed into a stainless-

https://doi.org/10.1021/acsomega.4c09975
ACS Omega 2025, 10, 16184−16193

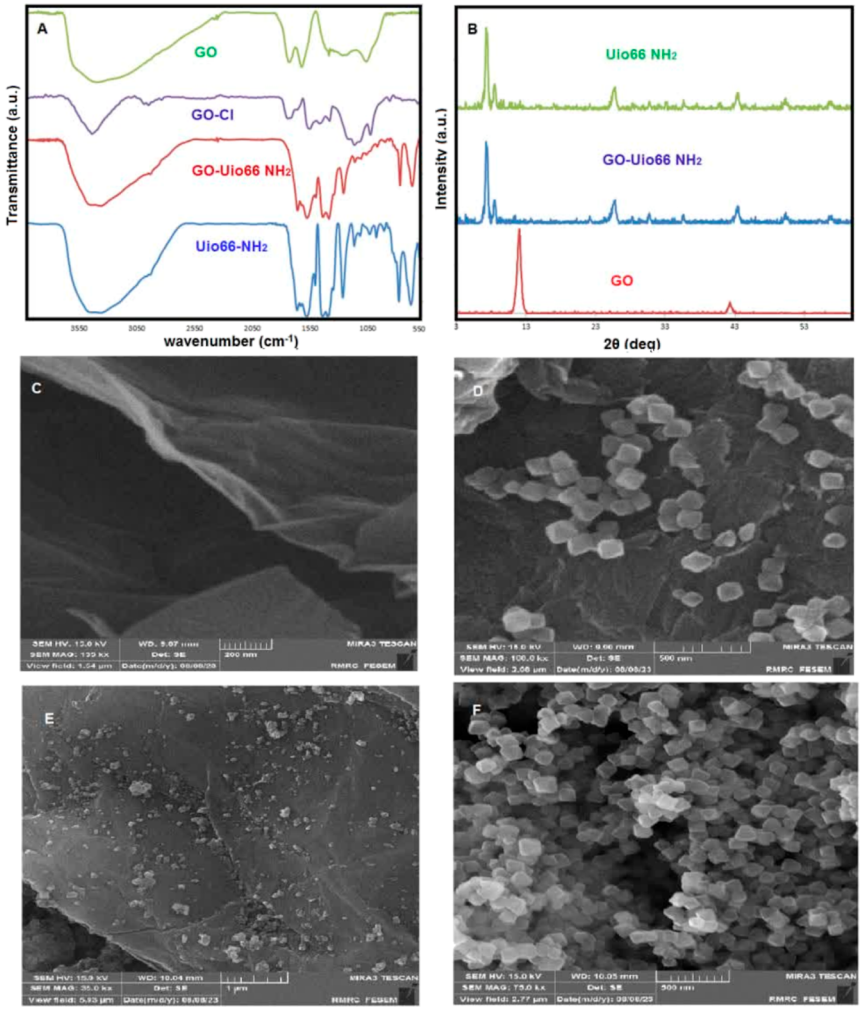

Figure 1. FT-IR spectra (A) and XRD patterns of synthesized products (B) and SEM images of GO (C), GO/UiO-66-NH_2 (D,E), and UiO-66-NH_2 (F).

steel grinding jar, equipped with 60 stainless-steel grinding balls with different diameters (3 × 20 balls, each with diameters of 3, 6, and 8 mm). The jar was then sealed and milled continuously for 40 min at a stirring rate of 200 rpm. In the next step, a mixture of zirconium acetate (1.8 g, 5.5 mmol) and NH_2−BDC (0.5, 2.76 mmol) were added afterward to the contents of the jar mill and milling process was continued at 200 rpm for another 40 min. The ball-to-powder mass ratio was consistently kept at about 24:1 for this experiment to ensure an efficient reaction. The resulting powder was gently washed with 30 mL of ethanol and DMF in a beaker by magnetic stirring for 3 h and after centrifugation dried in vacuum at 150 °C for 10 h. Similarly, UiO-66-NH_2 was prepared using the same way without the first step treatment.

2.4. Preparation of Modified Electrode. Prior to modification, the GCE was polished with 0.3 and 0.05 mm alumina slurries to remove adsorbed organic substances and then washed by sonication in ethanol and double distilled water. The prepared hybrid nanocomposite (10 mg) was dispersed in 1 mL of THF under sonication for 30 min. Then, 50 μL of a 10 mg mL^{-1} suspension was dropped onto the surface of GCE and dried under infrared light to prepare GO/UiO-66-NH_2/GCE.

2.5. Sample Preparation. Raw milk samples were obtained from a cattle farm, and other whole milk samples were prepared from local markets. All the samples were kept in a refrigerator at 2 °C before sample preparation. Prior to the handling of the raw milks, the samples were heated at 80 °C for 10 min to inactivate natural inhibitory substances (lysozymes). A volume of 20.0 mL milk sample was homogenized and mixed with 4 mL of 0.2 M Na_2EDT and 2.5 mL of 80% trichloroacetic acid in 50 mL polypropylene centrifuge tubes. Then, the mixture was centrifuged at 15,000 rpm for 60 min at 4 °C. The resultant supernatant was removed and then loaded to a C18 SPE cartridge, which had been previously activated with 6 mL of 50% methanol in deionized water at a flow rate of 3 mL/min, followed by rinsing with 2 mL of deionized water. The TC elution was carried out by 5 mL of HPLC grade methanol at a flow rate of 4 mL min^{-1}. Finally, the eluate was dried, and the residue was reconstituted with 25 mL of PBS for the DPV measurement under optimized conditions. The recovery studies were carried out by spiking the milk samples with TC standards at certain levels.

2.6. Electroanalytical Procedure. The three electrodes were immersed in the voltammetric cell, containing 25 mL of PBS (pH = 2.0). Then, an aliquot of the standard or sample solution was added to the cell, and the solution was magnetically stirred for 1 min at 400 rpm under open circuit conditions to facilitate TC adsorption onto the surface of the fabricated sensor. After 30 s (equilibration time), the DPV

https://doi.org/10.1021/acsomega.4c09975
ACS Omega 2025, 10, 16184−16193

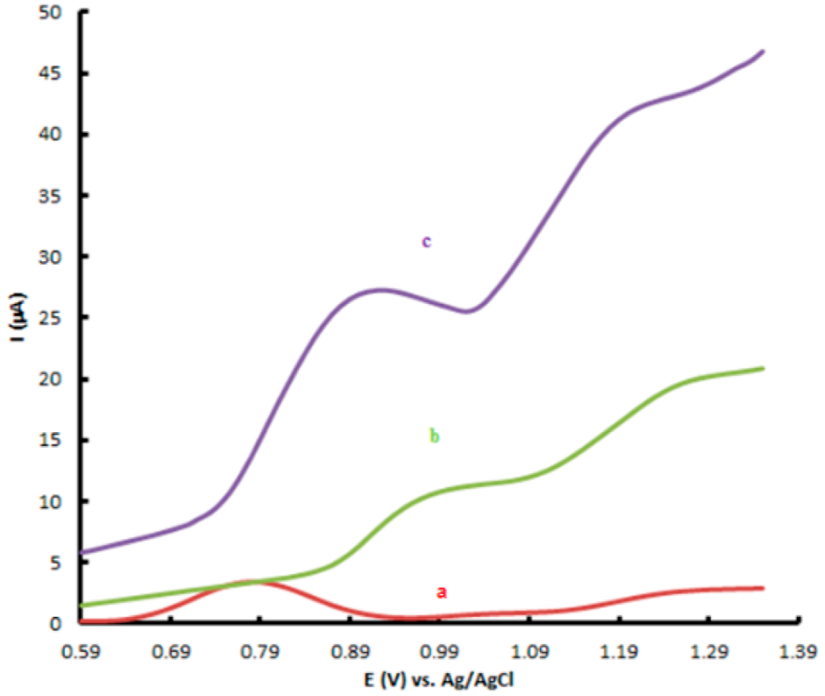

Figure 2. DPV voltammograms of TC at bare GO/GCE (a), UiO-66-NH_2/GCE (b), and GO/UiO-66-NH_2/GCE (c). Scan rate = 100 mV s^{-1}, equilibrium time = 1 min, step potential 7 mV, pulse amplitude = 30 mV, pulse period = 50 m s.

voltammograms were recorded over the potential range 0.64−1.3 V, utilizing a sweep rate of 150 mV s^{-1}, step potential of 0.025 V, pulse amplitude of 0.10 V, and pulse time of 50 ms. After each run, the fabricated sensor was washed with double distilled water and buffer solution (PBS, pH = 2.0). Also, after 5 consecutive runs, the modified GC electrode was repolished and again fabricated, as described above. All electrochemical measurements were carried out at room temperature.

3. RESULTS AND DISCUSSION

In this study, GO/UiO-66-NH_2 was selected as the main sensor recognition element because it represents an isotropic pore geometry and nanocomposite prototype with a specific single particle size, high monodispersity, good conductivity, and high affinity to TC via several effective interactions. Also, the mechanochemical synthesis method was selected as a green, fast, inexpensive, and one-pot strategy for the preparation of the GO/UiO-66-NH_2 hybrid nanocomposite with reliable repeatability and reproducibility. In addition, incorporation of GO into MOFs can improve the electrical conductivity of the sensor and also provide more active adsorption sites for TC. Also, acetate was selected as the counteranion of the metal precursor, because acetate anions, as an anion of an organic acid, may act as a Brønsted base in the reaction mixture and promote deprotonation of the carboxyl groups of the organic ligand. This can facilitate the coordination of the metal ion and organic ligand and promote the formation of MOFs.

3.1. Structural Characterization. FT-IR spectra of the GO, GO-Cl, UiO-66-NH_2, and GO/UiO-66-NH_2 are shown in Figure 1A. For GO, the O−H stretching at 3376 cm^{-1}, the O−H bending at 1384 cm^{-1}, the C═O stretching at 1732 cm^{-1}, and the characteristic C═C vibrations of the graphene skeleton around 1660 cm^{-1} can be seen. For GO-Cl, The absorption peak at 824 cm^{-1} is attributed to the C−Cl vibration band. This is close to the calculated single C−Cl vibration mode (A2u) at 850 cm^{-1}.[26] The FTIR spectra of GO/UiO-66-NH_2 shows similar characteristic peaks of UiO-66-NH_2. Also, the oxygen-containing functional peaks of GO show a decrease, which is ascribed to the coordination of the carboxyl groups of GO and Zr^{4+}. In the FTIR spectrum of GO/UiO-66-NH_2, the peaks at 3458 and 3361 cm^{-1} are attributed to the symmetrical and asymmetrical vibrations of −NH_2. The band at 1621 cm^{-1} is related to the N−H bending vibration. The peaks appearing at 1428 and 1373 cm^{-1} can be attributed to the N−H vibration and C−N stretching vibration of aromatic amine, respectively. Also two peaks at 670 and 768 cm^{-1} are assigned to the −NH_2 and −NH− groups. The characteristic peaks of GO disappeared in the GO/UiO-66-NH_2 composite because the oxygen-containing groups of the GO layer could bond with the amine groups and open metal sites of UiO-66-NH_2 in the composite. Furthermore, the characteristic broad bands of the hydroxyl group of the carboxylic moiety in the GO and the −NH_2 stretching band in UiO-66-NH_2 (around 3300−3500 cm^{-1}) have evolved into two weak broad bands at 3458 and 3390 cm^{-1}. The FT-IR spectrum of the composite is consistent with the reported ones that were synthesized by solvothermal and microwave methods.[27,28] XRD patterns of GO, UiO-66-NH_2, and GO/UiO-66-NH_2 are presented in Figure 1B. The pristine GO showed a sharp and strong diffraction peak at 2θ = 12.2°, indicating an interplanar distance of 0.819 nm. The synthesized GO/UiO-66-NH_2 nanocomposites have a good crystal structure and show the same diffraction peaks as UiO-66-NH_2 (CCDC no. 889529),[29] demonstrating that the incorporation of GO did not damage or change the UiO-66-NH_2 crystal structure. It should be noted that the characteristic peak of GO (2θ = 12.2°) does not appear in GO/UiO-66-NH_2 composites, indicating that low contents of GO are highly dispersed by intercalating UiO-66-NH_2 particles. According to the Scherrer equation, the crystal size of the GO/UiO-66-NH_2

https://doi.org/10.1021/acsomega.4c09975
ACS Omega 2025, 10, 16184−16193

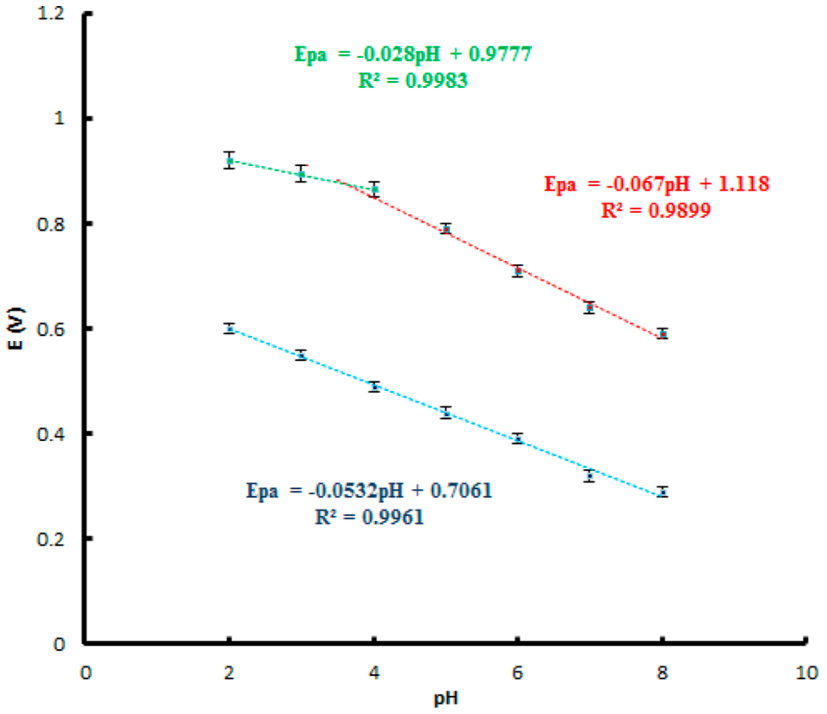

Figure 3. Effect of pH on the anodic peak potential of TC at the GO/UiO-66-NH_2/GCE. Error bars represent the standard deviation for three experiments.

hybrid nanocomposite was found to be 75 nm. SEM images of different samples are showed in Figure 1C−F. For GO, the characteristic wrinkled and layered structure of the metallic gray-colored surface of the graphene structure can be clearly observed. Also, for UiO-66-NH_2, distinctive cubic crystalline nanostructures were found. The high affinity of the oxygen-containing groups of the GO surface to coordinate with Zr^{4+} ions allows the surface of GO to act as an effective site for the nucleation and growth of MOF crystals. The SEM images of the hybrid composite (Figure 1D,E) indicated that the smooth surfaces of GO layers were homogeneously decorated with cubic crystals of UiO-66-NH_2. Due to the effect of synthesis conditions, the particle size of the GO/UiO-66-NH_2 composites was around 80−105 nm. The nanosize of synthesized composites could be attributed to the presence of GO. It has been shown that the combination of oxygen functional groups of GO with Zr^{4+} can inhibit the crystal growth of UiO-66-NH_2.[27]

3.2. Electrochemical Oxidation of TC at the Sensor. The oxidation responses of TC on the surface of GO, UiO-66-NH_2, and GO/UiO-66-NH_2 sensors were compared using DPV. As shown in Figure 2a, a relatively low peak current was obtained for GO, indicating that the oxidation activity of TC is poor on the GO surface. The oxidation peak of TC apparently enhanced at UiO-66-NH_2 (Figure 2b), due to the intrinsic high degree of porosity, large surface area, and better adsorption capacity of MOFs. The oxidation peak current increased by 2.5-fold at the surface of GO/UiO-66-NH_2 (Figure 2c), due to the increased conductivity caused by GO and also more available active adsorption sites for TC.

TC consists of a linear fused tetracyclic core with different functional groups (Figure S1). Several interactions can be considered between TC and GO/UiO-66-NH_2, including $\pi-\pi$ interactions, electrostatic interactions, and chemical coordination, which can improve the adsorption of TC on the sensor surface and provide plenty of electroactive sites for the TC oxidation. $\pi-\pi$ interactions can occur between electron-rich $-NH_2$ groups and benzene rings of TC, GO, and MOF. $\pi-$cation bonding can also be established in acidic media between amide groups and π-electron centers of TC, GO, and MOFs. Also, the nitrogenous groups of TC can replace the carboxylic groups of the MOF ligand and coordinate with Zr−O clusters. Also, the presence of GO leads to a decrease in the overpotential of the anodic peak compared to the pristine MOF. The meaningful increase in the peak current and negative shift of the peak potential shows that the GO/UiO-66-NH_2 sensor exhibits a strong synergistic enhancement effect toward the electron transfer of the system and oxidation of TC. The oxidation of TC can occur at the dimethylamino and phenolic groups. At acidic media, the dimethylamino group is protonated and, therefore, the phenolic group of the TC molecule is more likely to be oxidized. As can be seen (Figure 2c), TC exhibited two oxidation peaks around 0.92 and 1.19 V, which could be attributed to the oxidation of the phenolic group of TC with the subsequent addition of the hydroxyl group and the oxidation of the generated intermediate during the first oxidation step, respectively.[30] The current density of the first peak was higher than the second peak and, therefore, the first anodic peak was selected for the following experiments due to better sensitivity. Furthermore, the sensor showed no oxidation response for the blank, indicating the attribution of the oxidation peak to TC. Also, the ferricyanide/ferrocyanide ($Fe(CN)_6^{4-/3-}$) probe was used to compare the performance of UiO-66-NH_2 and GO/UiO-66-NH_2 sensors. Figure 3 shows the cyclic voltammograms of 0.01 mol L^{-1} $Fe(CN)_6^{4-/3-}$ in a 0.5 M KCl solution of two sensors at a scan rate of 150 mV s^{-1}. The value of peak separation ($\Delta E_p = E_{pa} - E_{pc}$) for the UiO-66-$NH_2$ and GO/UiO-66-NH_2 sensors were 65 and 42 mV, respectively. This could result from the improved electron-transfer kinetics at the GO/UiO-66-NH_2 sensor compared to

https://doi.org/10.1021/acsomega.4c09975
ACS Omega 2025, 10, 16184−16193

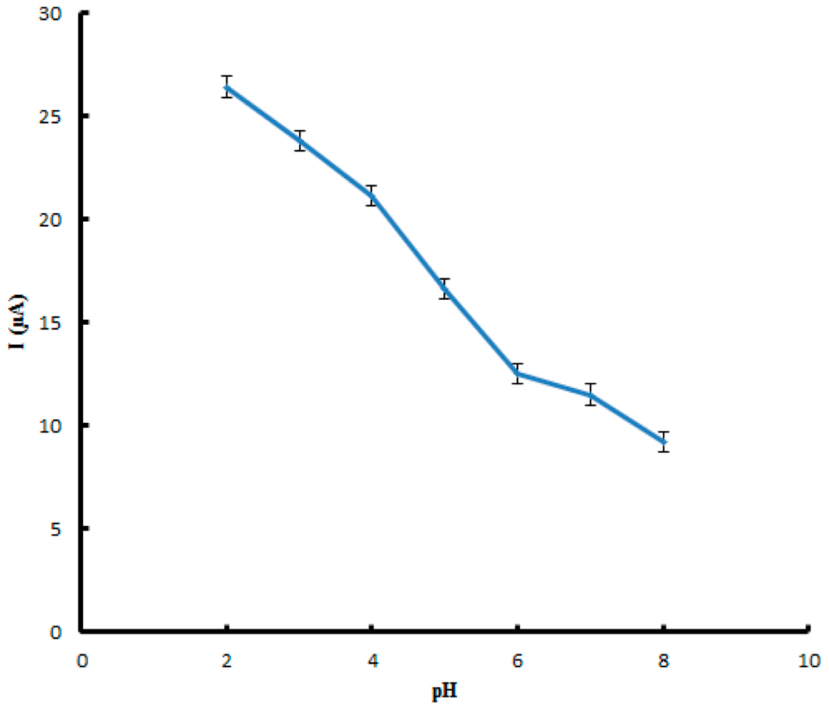

Figure 4. Effect of pH on the anodic peak current of TC at the GO/UiO-66-NH_2/GCE. Error bars represent the standard deviation for three experiments.

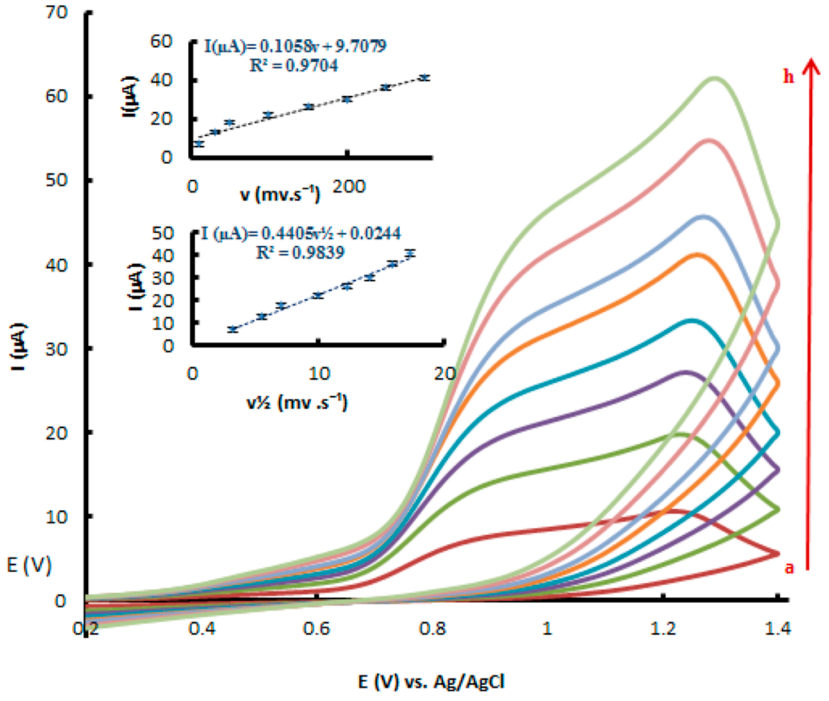

Figure 5. Cyclic voltammograms recorded at GO/UiO-66-NH_2/GCE for TC (pH 2.0) at different scan rates (from a to h: 25, 50, 75, 100, 150, 200, 250, and 300 mV s^{-1}). Inset: plot of I_p versus scan rate (υ) and square root of scan rates ($\upsilon^{1/2}$).

UiO-66-NH_2. The better electron-transfer capability and better reversibility of GO/UiO-66-NH_2 than UiO-66-NH_2 for the ferricyanide/ferrocyanide redox pair demonstrated that the GO/UiO-66-NH_2 hybrid composites exhibited a remarkably better electrochemical performance than that of the UiO-66-NH_2.

3.3. Effect of pH. The effect of pH on the electrooxidation of 4 μg L^{-1} TC was studied over the pH range of 2.0−8.0 (Figure S2). The results (Figure 3) showed that the peak potentials (E_{pa}, V) of TC presented a negative shift with increasing pH, indicating the involvement of protons in the oxidation reactions.

For the first anodic peak, E_{pa} and pH showed a linear relationship (Figure 3) with regression equation $E_{pa} = -0.0532$ pH + 0.7061 (R^2 = 9961). The slope value of around 53 mV pH^{-1} indicates that the same number of electrons and protons

https://doi.org/10.1021/acsomega.4c09975
ACS Omega 2025, 10, 16184−16193

are involved in TC oxidation on the surface of the proposed sensor. For the second oxidation peak, two linear relationships were found over pH ranges 2−4 and 4−8 (Figure 3), with regression equations E_{pa} = −0.028 pH + 0.9777 (R^2 = 9983) and E_{pa} = 0.067 pH + 1.118 (R^2 = 0.9899), respectively. The slopes of 0.028 and 0.067 mV pH $^{-1}$ can be attributed to the involvement of one proton and two electrons (pH = 2−4) and the same number of protons and electrons (pH = 4−8) in the redox process of TC, which is consistent with previous reports.[30−32] Also, the oxidation peak current decreased with increasing pH (Figure 4). Considering the sensitivity of the determination of TC, the pH of 2.0 was selected as the optimum value.

3.4. Effect of Scan Rate. The effect of the scan rate on the electrochemical response of GO/UiO-66-NH_2 for 4 μg mL^{-1} TC was investigated using the CV technique. The recorded voltammograms (Figure 5) showed that the current intensities are increased with the increase of the scan rates. Also, a positive shift was observed for oxidation peak potential with increasing scan rates, confirming the irreversibility of the TC oxidation reaction. Furthermore, the curves of I (μA) versus scan rates (υ, mV s^{-1}) and square root of scan rates ($\upsilon^{1/2}$, [mVs^{-1}]$^{1/2}$) were plotted (Figure 5). Good linear relationships were found for both with regression equations of I_{pa} = 0.1058 ν + 9.708 (R^2 = 0.9704) and I_{pa} = 0.4405$\nu^{1/2}$ + 0.0244 (R^2 = 0.9839), respectively. This shows that TC oxidation at GO/UiO-66-NH_2 is controlled by both diffusion and adsorption mechanisms.

3.5. Analytical Performance. The analytical parameters of the fabricated sensor were investigated under the optimized conditions (Table S1). As can be seen in Figure 6, the

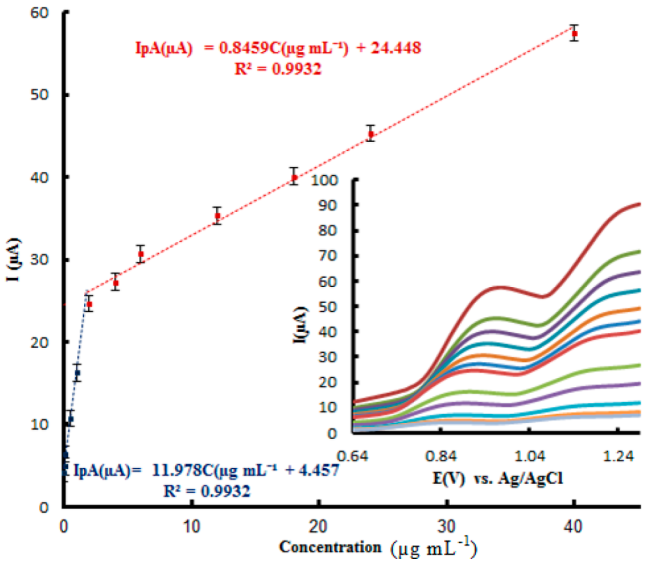

Figure 6. DPV responses for different concentrations of TC under optimized conditions (A); calibration graph achieved from DPV measurements. Error bars represent the standard deviation for three experiments.

oxidation peak current (I_{pa}) of TC increased correspondingly with the increasing TC concentration. A linear relationship was found over two concentration ranges of 0.02−1.00 and 1.00−40.00 μg mL^{-1} with the regression equations I_{pa} (μA) = 11.98C (μg mL^{-1}) + 4.457 (R^2 = 0.9921) and I_{pa} (μA) = 0.8459C (μg mL^{-1}) + 24.45 (R^2 = 0.9932), respectively.

The limit of detection (LOD) calculated as LOD = $3S_b/m$ (where, S_b and m are the standard deviation of the blank signal and the slope of the calibration graph, respectively) was found to be 0.003 μg mL^{-1}. This is significantly lower than the maximum residue limit (100 ng mL^{-1}) for TC in milk samples, as defined by the World Health Organization (WHO) and European Medicines Agency and Committee for Medicinal Products for veterinary Use (EMA-CVMP).[32−34] The repeatabilities of the proposed sensor, as the relative standard deviation for five replicate measurements of 0.5 and 4 μg mL^{-1}of TC using the same sensor, were 3.8 and 3.1%, respectively. The reproducibility of this sensor as the RSD value of five separate measurements of 4 μg mL^{-1} of TC with five fabricated sensors prepared on different days was 4.8%. For evaluating the stability of the sensor, the sensor was kept at room temperature for 3 weeks and then used for TC determination. The results showed that the oxidation peak current value retained 94.6% of the initial response and the peak potential remained almost unchurched, indicating the long-term stability of the sensor. A comparison of the analytical properties of the proposed sensor and other reported sensors is shown in Table 1.

The proposed sensor provides evident advantages such as a wider linear concentration range, lower detection limit, and better sensitivity.

3.6. Interference Study. To investigate the selectivity of the proposed sensor, the effect of various possible interferences on the determination of TC was evaluated. The tolerance level was defined as the amount of the investigated species causing a change of +5% in the signal intensity using a sample solution containing 4 μg mL^{-1} TC. The results show that 500-fold Na^+, Ca^{2+}, Mg^{2+}, Fe^{3+}, Al^{3+}, Cl^-, SO_4^{2-}, PO_4^{3-}, CO_3^{2-}, 200-fold sucrose, glucose, glycine, vanillin, oleic acid, and 20-fold ascorbic acid and citric acid showed no interference on the TC response. The interferences of some common antibiotics are also tested. 20-fold ampicillin, penicillin, chloramphenicol, erythromycin, amoxicillin, and 12-fold oxytetracycline showed no interference on the TC response. Electrochemical sensors are very sensitive toward surface active materials, such as proteins and amino acids in food samples. Thus, the effects of some typical surface active species such as bovine serum albumin (BSA), serine (SE), aspartic acid (AA), glutamic acid (GA), and L-tyrosine (LT) on the behavior of TC were evaluated. The results showed that 50-fold BSA and 100-fold SE, AA, GA, and LT have no influence on the TC oxidation current. Thus, the presented sensor affords a good anti-interference ability and is suitable for TC detection in real samples with various matrices.

3.7. Analysis of Real Samples. The applicability and reliability of the proposed sensor were investigated by the determination of TC in different milk samples (Table 2). Recovery studies were performed by spiking milk samples with different amounts of TC. The found relative recovery values were in the range of 94.0−105.0%, confirming acceptable performance of the sensor for TC analysis in real samples. Furthermore, the accuracy of the presented sensor was checked by the official HPLC procedure.[42]

Comparison of the results (Table 3) through the paired Student's t test and F-test at a 95% confidence level showed no statistically meaningful difference between the results of the two methods with respect to accuracy and precision. These investigations demonstrated that the suggested sensor could be

https://doi.org/10.1021/acsomega.4c09975
ACS Omega 2025, 10, 16184−16193

Table 1. Comparison of Different Analytical Methods for TC Determination

sensor[a]	detection[b]	linear range μg mL^{-1}	LOD μg mL^{-1}	sample	refs
GR/l-Cys/GCE	DPV	3.55−62.22	0.089	water	35
MWCNT−COOH−GO/CPE	AdSDPV	8.89−137.77	0.160	water, urine, pharmaceutical	36
AGC	DPV	0.89−7.11	0.102	pork	37
		7.11−36.89			
GPUE-MIP-TC	DPASV	1.77−17.78	1.24	artificial urine, pharmaceutical	38
Ni-GCCME	FI-Amper	2.5−80.0	0.03	pharmaceutical	39
Fe/Zn−MMT/GCE	DDPV	0.13−23.1	0.04	feedstuff, meat	40
ERGO/SPE	AdTDPV	8.88−35.55	5.33	milk, water	41
GO/UiO66-NH_2/GCE	DPV	0.02−1.00	0.003	milk	this work
		1.00−40.00			

[a]GR/L-Cys/GCE: graphene/L-cysteine/GCE; MWCNT−COOH−GO/CPE/multiwalled carbon nanotube-functionalized-graphene oxide/carbon paste electrode; AGC: activated glassy carbon; GPUE-MIP-TC: graphite-polyurethane composite electrode modified molecularly imprinting polymer containing tetracycline; Ni-GCCME: nickel-modified glassy carbon electrode ; FI-amper: flow injection amperometry; Fe/Zn−MMT/GCE: iron/zinc-cation exchanged montmorillonite/glassy carbon electrode; ERGO/SPE: electrochemical reduced graphene oxide/screen-printed electrode. [b]DPV: differential pulse voltammetry; AdSDPV: adsorptive stripping differential pulse voltammetry; DPVASV: differential pulse anodic stripping voltammetry; DDPV: derivative differential pulse voltammetry; AdTDPV: adsorptive transfer stripping differential pulse voltammetry.

Table 2. Result for TC Determination in Real Samples

sample	spiked (ng mL^{-1})	found (ng mL−1)	recovery (%)
cow milk		ND[a]	
	0.50	0.48 ± 0.04[b]	96.0
	4.00	4.20 ± 0.03	105.0
goat milk		ND	
	0.50	0.47 ± 0.03	94.0
	4.00	3.90 ± 0.04	97.5
cow pasteurized milk		ND	
	0.50	0.49 ± 0.03	98.0
	4.00	4.10 ± 0.02	102.5

[a]Not detected. [b]Mean of five measurement ± standard deviation.

Table 3. Comparison of TC Analyses in Spiked Milk Samples by the Proposed Sensor and Reference Method (Results: Mean ± Standard Deviation, n = 3)

		found (μg mL^{-1})	
sample	added (μg mL^{-1})	sensor	HPLC
cow milk	0.00	ND[a]	ND
	0.50	0.48 ± 0.04	0.49 ± 0.01
	4.00	4.20 ± 0.03	4.10 ± 0.05

[a]ND: Not detected.

used to determine trace amounts of TC in milk samples with acceptable accuracy and validity.

4. CONCLUSIONS

In this work, a sensitive electrochemical sensor was fabricated for the determination of TC residual in milk samples based on the GO/UiO-66-NH_2 hybrid nanocomposite. An easy, rapid, low cost, solvent-free, and room-temperature milling procedure was developed for the synthesis of the GO/UiO66-NH_2 nanocomposite. The unique features like high surface area, high porosity, and active adsorption sites can improve the performance of the sensor for TC determination. The high adsorption capacity can be attributed to different possible interactions such as N-π and $\pi-\pi$ stacking interactions, acid−base interactions, and hydrogen bonding interactions. The proposed sensor showed a good sensitivity, low detection limits, and superior analytical performance for TC analysis in milk samples. Moreover, the fabricated sensor presents a low detection limit, which is remarkably lower than the maximum residue limit set by both the WHO and EMA−CVMP in milk samples. The proposed sensor was successfully used for TC determination in various milk samples with acceptable recoveries (94.0−105.0%).

■ ASSOCIATED CONTENT

Supporting Information

The Supporting Information is available free of charge at https://pubs.acs.org/doi/10.1021/acsomega.4c09975.

TC structure, recorded voltammograms in different pH, and table of analytical parameters (PDF)

■ AUTHOR INFORMATION

Corresponding Author

Mahdi Hashemi − *Department of Analytical Chemistry, Faculty of Chemistry and Petroleum Sciences, Bu-Ali Sina University, Hamedan 6515733677, Iran;* orcid.org/0000-0002-8907-8036; Phone: +98-8138380709; Email: mhashemi@basu.ac.ir

Author

Davood Bigdelifam − *Department of Analytical Chemistry, Faculty of Chemistry and Petroleum Sciences, Bu-Ali Sina University, Hamedan 6515733677, Iran*

Complete contact information is available at: https://pubs.acs.org/10.1021/acsomega.4c09975

Author Contributions

D.B.: Writing—original draft, Conceptualization, Methodology, Investigation, Data curation, Formal analysis; M.H.: Writing—review and editing, Validation, Supervision, Methodology, Funding acquisition.

Notes

The authors declare no competing financial interest.

■ ACKNOWLEDGMENTS

We are pleased to acknowledge the support of this work by Bu-Ali Sina University Research Council.

REFERENCES

(1) Sachi, S.; Ferdous, J.; Sikder, M. H.; Hussani, S. M. A. K. Antibiotic residues in milk: Past, present, and future. *J. Adv. Vet. Anim. Res.* **2019**, *6* (3), 315−332.

(2) Meyer, M. T.; Bumgarner, J. E.; Varns, J. L.; Daughtridge, J. V.; Thurman, E. M.; Hostetler, K. A. Use of radioimmunoassay as a screen for antibiotics in confined animal feeding operations and confirmation by liquid chromatography/mass spectrometry. *Sci. Total Environ.* **2000**, *248* (2−3), 181−187.

(3) Ahmadijokani, F.; Molavi, H.; Tajahmadi, S.; Rezakazemi, M.; Amini, M.; Kamkar, M.; Rojas, O. J.; Arjmand, M. Cordination chemistry of metal−organic frameworks: Detection, adsorption, and photodegradation of tetracycline antibiotics and beyond. *Coord. Chem. Rev.* **2022**, *464*, 214562.

(4) Kirchhelle, C. Pharming animals: A global history of antibiotics in food production (1935−2017). *Palgrave Commun.* **2018**, *4* (1), 1−13.

(5) Fonseca, G. P.; Cruz, A. G.; Faria, J. A. F.; Silva, R.; Moura, M. R. L.; Carvalho, L. M. J. Antibiotic residues in Brazilian UHT milk: a screening study. *Food Sci. Technol.* **2009**, *29* (2), 451−453.

(6) Alipour, F.; Mirlohi, M.; Jalali, M.; Azadbakht, L. Dietary exposure to tetracycline residues through milk consumption in Iran. *J. Environ. Health Sci. Eng.* **2015**, *13* (80), 1−7.

(7) WHO Technical Report Series. *Evaluation of Certain Veterinary Drug Residues in Food (Fiftieth Report of the Joint FAO/WHO Expert Committee on Food Additives)*, 1999; *888*.

(8) Önal, A. Overview on liquid chromatographic analysis of tetracycline residues in food matrices. *Food Chem.* **2011**, *127* (1), 197−203.

(9) Vuran, B.; Ulusoy, H. I.; Sarp, G.; Yilmaz, E.; Morgül, U.; Kabir, A.; Tartaglia, A.; Locatelli, M.; Soylak, M. Determination of chloramphenicol and tetracycline residues in milk samples by means of nanofiber coated magnetic particles prior to high-performance liquid chromatography-diode array detection. *Talanta* **2021**, *230*, 122307.

(10) Zergiebel, S.; Ueberschaar, N.; Seeling, A. Development and optimization of an ultra-fast microextraction followed by HPLC-UV of tetracycline residues in milk products. *Food Chem.* **2023**, *402*, 134270.

(11) Igualada, C.; Giraldo, J.; Font, G.; Yusà, V. Validation of a multi-residue UHPLC-HRMS method for antibiotics screening in milk, fresh cheese, and whey. *J. Food Compos. Anal.* **2022**, *106*, 104265.

(12) Chen, J.; Ying, G.-G.; Deng, W.-J. Antibiotic residues in food: Extraction, analysis, and human health concerns. *J. Agric. Food Chem.* **2019**, *67* (27), 7569−7586.

(13) Lanjwani, M. F.; Altunay, N.; Tuzen, M. Preparation of fatty acid-based ternary deep eutectic solvents: Application for determination of tetracycline residue in water, honey and milk samples by using vortex-assisted microextraction. *Food Chem.* **2023**, *400*, 134085.

(14) Hu, D.; Jiang, S. Z.; Xia, T.; Xiao, D.; Li, Y.; Hou, Y.; Zhang, J. Z.; Pu, Y.-C. Enhanced fluorescence sensing of tetracycline with Ti2C quantum dots. *Nano Res.* **2024**, *17*, 3180−3188.

(15) Zhou, L.; Li, D.-J.; Gai, L.; Wang, J. P.; Li, Y.-B. Electrochemical aptasensor for the detection of tetracycline with multi-walled carbon nanotubes amplification. *Sens. Actuators, B* **2012**, *162* (1), 201−208.

(16) Guo, G.; Zhao, F.; Xiao, F.; Zeng, B. Voltammetric determination of tetracycline by using multi-wall carbon nanotube − ionic liquid film coated glassy carbon electrode. *Int. J. Electrochem. Sci.* **2009**, *4* (9), 1365−1372.

(17) Devkota, L.; Nguyen, L. T.; Vu, T. T.; Piro, B. Electrochemical determination of tetracycline using AuNP-coated molecularly imprinted overoxidized polypyrrole sensing interface. *Electrochim. Acta* **2018**, *270*, 535−542.

(18) Geleta, G. S. Recent advances in electrochemical sensors based on molecularly imprinted polymers and nanomaterials for detection of ascorbic acid, dopamine, and uric acid: A review. *Sens. Biosensing Res.* **2024**, *43*, 100610.

(19) Baranwal, J.; Barse, B.; Gatto, G.; Broncova, G.; Kumar, A. Electrochemical sensors and their applications: A review. *Chemosensors* **2022**, *10* (9), 363.

(20) Daniel, M.; Mathew, G.; Anpo, M.; Neppolian, B. MOF based electrochemical sensors for the detection of physiologically relevant biomolecules: An overview. *Coord. Chem. Rev.* **2022**, *468*, 214627.

(21) Wu, M.; Zhang, Q.; Zhang, Q.; Wang, H.; Wang, F.; Liu, J.; Guo, L.; Song, K. Research progress of UiO-66-Based electrochemical biosensors. *Front. Chem.* **2022**, *10*, 842894.

(22) Saha, R.; Gupta, K.; García, C. J. G. Strategies to improve electrical conductivity in metal−organic frameworks: A comparative study. *Cryst. Growth Des.* **2024**, *24* (5), 2235−2265.

(23) Li, Z.; Liu, C.; Frick, J. J.; Davey, A. K.; Dods, M. N.; Carraro, C.; Senesky, D. G.; Maboudian, R. Synthesis and characterization of UiO-66-NH_2 incorporated graphene aerogel composites and their utilization for absorption of organic liquids. *Carbon* **2023**, *201*, 561−567.

(24) Užarević, K.; Wang, T. C.; Moon, S.-Y.; Fidelli, A. M.; Hupp, J. T.; Farha, O. K.; Friščić, T. Mechanochemical and solvent-free assembly of zirconium-based metal−organic frameworks. *Chem. Commun.* **2016**, *52* (10), 2133−2136.

(25) Do, J. L.; Friščić, T. Mechanochemistry: A force of synthesis. *ACS Cent. Sci.* **2017**, *3* (1), 13−19.

(26) Bouša, D.; Luxa, J.; Mazanek, V.; Jankovsky, O.; Sedmidubsky, D.; Klímová, K.; Pumera, M.; Sofer, Z. Toward graphene chloride: chlorination of graphene and graphene oxide. *RSC Adv.* **2016**, *6* (71), 66884−66892.

(27) Cao, Y.; Zhang, H.; Song, F.; Huang, T.; Ji, J.; Zhong, Q.; Chu, W.; Xu, Q. UiO-66-NH_2/GO Composite: Synthesis, Characterization and CO_2 Adsorption Performance. *Materials* **2018**, *11* (4), 589.

(28) Ning, H.; Yang, Z.; Yin, Z.; Wang, D.; Meng, Z.; Wang, C.; Zhang, Y.; Chen, Z. A novel strategy to enhance the performance of CO_2 adsorption separation: Grafting hyper-cross-linked polyimide onto composites of UiO-66-NH_2 and GO. *ACS Appl. Mater. Interfaces* **2021**, *13* (15), 17781−17790.

(29) Kazemi, A.; Moghadaskhou, F.; Pordsari, M. A.; Manteghi, F.; Tadjarodi, A.; Ghaemi, A. Enhanced CO_2 capture potential of UiO-66-NH_2 synthesized by sonochemical method: experimental findings and performance evaluation. *Sci. Rep.* **2023**, *13*, 19891.

(30) Kushikawa, R. T.; Silva, M. R.; Angelo, A. C. D.; Teixeira, M. F. S. Construction of an electrochemical sensing platform based on platinum nanoparticles supported on carbon for tetracycline determination. *Sens. Actuators, B* **2016**, *228*, 207−213.

(31) Calixto, C. M. F.; Cervini, P.; Cavalheiro, E. ⸗. T. G. Determination of tetracycline in environmental water samples at a graphite-polyurethane composite electrode. *J. Braz. Chem. Soc.* **2012**, *23* (5), 938−943.

(32) World Health Organization. Maximum residue limits (MRLs) and risk management recommendations (RMRs) for residues of veterinary drugs in foods. Codex Alimentarius Commission, WHO Technical Report Series; 38th session. 2015, www.fao.org/input/download/standards/45/MRL22015e.pdf. (accessed Jul 30, 2018).

(33) European Medicines Agency and Committe for Medicinal Products for Veterinary Use. Pharmacologically active substances and their classification regarding maximum residue limits in foodstuffs of animal origin. 2010R0037-EN-12.12.2010−002.001−1. London,UK. 2010, https://ec.europa.eu/health//sites/health/files/files/mrl/mrl20101212consol.pdf. (accessed Jul 30, 2018).

(34) Cramer, G.; Solano, L.; Johnson, R. Evaluation of tetracycline in milk following extra-label administration of topical tetracycline for digital dermatitis in dairy cattle. *J. Dairy Sci.* **2019**, *102* (1), 883−895.

(35) Sun, X.-M.; Ji, Z.; Xiong, M.-X.; Chen, W. The electrochemical sensor for the determination of tetracycline based on graphene /L-Cysteine composite film. *J. Electrochem. Soc.* **2017**, *164* (4), B107−B112.

(36) Wong, A.; Scontri, M.; Materon, E. M.; Lanza, M. R. V.; Sotomayor, M. D. P. T. Development and application of an electrochemical sensor modified with multi-walled carbon nanotubes

https://doi.org/10.1021/acsomega.4c09975
ACS Omega 2025, 10, 16184−16193

and graphene oxide for the sensitive and selective detection of tetracycline. *J. Electroanal. Chem.* **2015**, *757*, 250−257.
(37) Huong, N. T.; Hien, N. T. M.; Thuy, T. T. D.; Ai, N. T. N.; Anh, L. D. Q. Determination of tetracycline residue in pork by differential pulse voltammetry using activated glassy carbon electrode. *Vietnam J. Chem.* **2023**, *61* (1), 65−73.
(38) Clarindo, J. E. S.; Viana, R. B.; Cervini, P.; Silva, A. B.; Cavalheiro, E. T. G. Determination of tetracycline using a graphite-polyurethane composite electrode modified with a molecularly imprinted polymer. *Anal. Lett.* **2020**, *53* (12), 1932−1955.
(39) Oungpipat, W.; Southwell-Keely, P.; Alexander, P. W. Flow injection detection of tetracyclines by electrocatalytic oxidation at a nickel-modified glassy carbon electrode. *Analyst* **1995**, *120* (5), 1559−1565.
(40) Gan, T.; Shi, Z.; Sun, J.; Liu, Y. Simple and novelel ectrochemical sensor for the determination of tetracycline based on iron/zinc cations−exchanged montmorillonite catalyst. *Talanta* **2014**, *121*, 187−193.
(41) Lorenzetti, A. S.; Sierra, T.; Domini, C. E.; Lista, A. G.; Crevillen, A. G.; Escarpa, A. Electrochemically reduced graphene oxide-based screen-printed electrodes for total tetracycline determination by adsorptive transfer stripping differential pulse voltammetry. *Sensors* **2020**, *20* (1), 76.
(42) Carson, M. C.; Breslyn, W.; Carmany, J.; Cross, S.; Farrington, W. H.; Hahn, A.; Jaworski, J.; Lansdon, P.; Li, M.; Pearson, D.; et al. Simultaneous determination of multiple tetracycline residues in milk by metal chelate affinity chromatography: collaborative study. *J. AOAC Int.* **1996**, *79* (1), 29−42.

https://doi.org/10.1021/acsomega.4c09975
ACS Omega 2025, 10, 16184−16193